

# Finite Element Investigation of Damage on KFRP/CFRP Composite Laminates under Low-Velocity Impact

K. Suwanpakpraek and B. Patamaprohms

Department of Mechanical and Aerospace Engineering, Faculty of Engineering, King Mongkut's University of Technology North Bangkok, Bangkok, Thailand

Email: {k.suwanpakpraek@gmail.com, baramee.p@eng.kmutnb.ac.th}

**Abstract**—This study deals with damage investigation on KFRP/CFRP composite laminates subjected to low-velocity impact using a drop-weight impact test. The three variations of composite laminates including KFRP, CFRP and KFRP-CFRP composite laminates were tested. The results from KFRP and CFRP composite laminates were used to estimate the fracture energy of each material for KFRP-CFRP composite simulation. The goal is to model the complicated failure surface of KFRP-CFRP composite laminates using damage evolution models and also cohesive elements for interfacial failure between different composites. A good agreement with experimental results was found.

**Index Terms** –Kevlar Fiber Reinforced Polymers (KFRP), Carbon Fiber Reinforced Polymers (CFRP), Finite Element Method (FEM), Low-velocity impact

## I. INTRODUCTION

Currently, a weight reduction concept has been playing an important role in modern automotive design. A lower weight will decrease an energy consumption of modern automobiles. The successive and efficient way to reduce automobiles weight is to use various type of fiber-reinforced polymer composites (FRP) in body and structural parts. These materials have a high strength to weight ratio, knowing as a specific strength, especially a carbon fiber-reinforce polymer (CFRP) composite [1]. However, automobile composite parts are prone to impact load during regular use and also from some dropped tools during maintenance services which are classified as a low-velocity impact load [2]. As a brittle material, when CFRP is under an impact load, it can be damaged leading to delamination and fiber breaks, the important damage modes that degrade significantly strength of composite. Among other conventional FRPs, a Kevlar fiber-reinforce polymer (KFRP) composite is clearly superior than the others for supporting an impact load because of its very high tenacity [3]. The application of Kevlar ranging from cut-resistance gloves to bulletproof composites. Comparing to CFRP composites, the KFRP composites is still underneath in terms of specific strength and modulus which are important properties for composite structural components. Therefore, a KFRP-CFRP composite

laminate was studied in this work. A drop weight impact test was performed as a low-velocity impact load. The corresponding impact energy can be varied though the height of impactor. The failure surface of the KFRP-CFRP composite laminate shows a mix of composite failure mode including fiber breakage, matrix cracking and also delamination between KFRP and CFRP plies. This work intended to investigate this failure surface using finite element simulation. The model was taken into account an orthotropic behavior of composites, a non-linear behavior of KFRP, damage evolution models and also cohesive elements for delamination between different composite laminates.

## II. MATERIALS AND BEHAVIOR MODELS

The fiber fabric used in this study is a symmetric (50-50) 3k plain weave woven fabric for both Kevlar and carbon fiber. The composite laminates were fabricated by hand lay-up method using epoxy resin as a matrix. In general, the mechanical behavior of composites is orthotropic that can be described as in eq.1 where  $\sigma_{ij}$ ,  $\epsilon_{ij}$  are stress and strain tensor,  $[S]$  is a compliance matrix and  $E$ ,  $\nu$ ,  $G$  are elastic constants. For composites, the direction 1 always represents a fiber direction or warp direction in case of woven fabric composites. The direction 2 is a weft direction and the direction 3 is normal to composite plates. For symmetrical fabric composites, their behavior can be simplified as in-plan isotropic where  $E_{11}=E_{22}$ ,  $\nu_{13}=\nu_{23}$  and  $G_{13}=G_{23}$ .

$$\epsilon_{ij} = [S]\sigma_{ij} \tag{1}$$

$$\begin{Bmatrix} \epsilon_{11} \\ \epsilon_{22} \\ \epsilon_{33} \\ \gamma_{23} \\ \gamma_{13} \\ \gamma_{12} \end{Bmatrix} = \begin{bmatrix} \frac{1}{E_{11}} & -\frac{\nu_{21}}{E_{22}} & -\frac{\nu_{31}}{E_{33}} & 0 & 0 & 0 \\ -\frac{\nu_{12}}{E_{11}} & \frac{1}{E_{22}} & -\frac{\nu_{32}}{E_{33}} & 0 & 0 & 0 \\ -\frac{\nu_{13}}{E_{11}} & -\frac{\nu_{23}}{E_{22}} & \frac{1}{E_{33}} & 0 & 0 & 0 \\ 0 & 0 & 0 & \frac{1}{G_{23}} & 0 & 0 \\ 0 & 0 & 0 & 0 & \frac{1}{G_{13}} & 0 \\ 0 & 0 & 0 & 0 & 0 & \frac{1}{G_{12}} \end{bmatrix} \begin{Bmatrix} \sigma_{11} \\ \sigma_{22} \\ \sigma_{33} \\ \sigma_{23} \\ \sigma_{13} \\ \sigma_{12} \end{Bmatrix}$$

Manuscript received August 14, 2021; revised January 14, 2022.

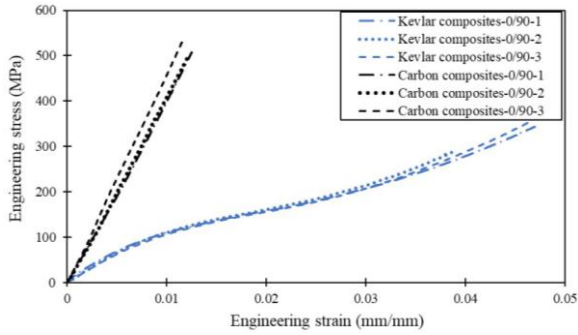


Figure 1. Comparison of tensile tests between CFRP and KFRP composites

Since the KFRP composite show an obvious non-linear behavior in comparison to the CFRP composite (Fig.1). Therefore, the anisotropic yield criterion with ductile damage were applied to material model of KFRP taking into account this non-linearity. This yield criterion is based on von Mises yield criterion and widely uses for metals, polymers, and certain composites (eq.2) [4].

$$f(\sigma) = \sqrt{\begin{matrix} H(\sigma_{11} - \sigma_{22})^2 + F(\sigma_{22} - \sigma_{33})^2 \\ + G(\sigma_{33} - \sigma_{11})^2 + 2N\sigma_{12}^2 \\ + 2M\sigma_{13}^2 + 2L\sigma_{23}^2 \end{matrix}} \quad (2)$$

where

$$H = \frac{1}{2} \left( \frac{1}{R_{11}^2} + \frac{1}{R_{22}^2} - \frac{1}{R_{33}^2} \right), F = \frac{1}{2} \left( \frac{1}{R_{22}^2} + \frac{1}{R_{33}^2} - \frac{1}{R_{11}^2} \right),$$

$$G = \frac{1}{2} \left( \frac{1}{R_{33}^2} + \frac{1}{R_{11}^2} - \frac{1}{R_{22}^2} \right), N = \frac{3}{2R_{12}^2}, M = \frac{3}{2R_{13}^2}, L = \frac{3}{2R_{23}^2}$$

and

$$R_{11} = \frac{\bar{\sigma}_{11}}{\sigma^0}, R_{22} = \frac{\bar{\sigma}_{22}}{\sigma^0}, R_{33} = \frac{\bar{\sigma}_{33}}{\sigma^0}, R_{12} = \frac{\bar{\sigma}_{12}}{\tau^0},$$

$$R_{13} = \frac{\bar{\sigma}_{13}}{\tau^0}, R_{23} = \frac{\bar{\sigma}_{23}}{\tau^0}$$

where  $\bar{\sigma}_{ij}$  is the measured yield stress,  $\sigma^0$  is the reference yield stress to define a plasticity of material and  $\tau^0 = \sigma^0 / \sqrt{3}$ . Concerning to the CFRP composite, its failure is clearly a brittle material which compatible with Hashin damage model. In this work, the 2D Hashin failure criteria was applied in the simulations. This version neglects out-of-plane stresses and can be only simulated with shell element under plan stress assumption. As a result, the delamination mode is lacking in this model. The fiber and matrix failure modes for both of tension and compression load [4] are described by

Fiber Tension ( $\sigma_{11} > 0$ ):

$$\left( \frac{\sigma_{11}}{X^T} \right)^2 + \alpha \left( \frac{\sigma_{12}}{S^L} \right) = \begin{cases} \geq 1 & \text{failure} \\ < 1 & \text{no failure} \end{cases} \quad (3)$$

Fiber Compression ( $\sigma_{11} < 0$ ):

$$\left( \frac{\sigma_{11}}{X^C} \right)^2 = \begin{cases} \geq 1 & \text{failure} \\ < 1 & \text{no failure} \end{cases} \quad (4)$$

Matrix Tension ( $\sigma_{22} > 0$ ):

$$\left( \frac{\sigma_{22}}{Y^T} \right)^2 + \left( \frac{\sigma_{12}}{S^L} \right)^2 = \begin{cases} \geq 1 & \text{failure} \\ < 1 & \text{no failure} \end{cases} \quad (5)$$

Matrix Compression ( $\sigma_{22} < 0$ ):

$$\left( \frac{\sigma_{22}}{2S^T} \right)^2 + \left[ \left( \frac{Y^C}{2S^T} \right)^2 - 1 \right] \frac{\sigma_{22}}{Y^C} + \left( \frac{\sigma_{12}}{S^L} \right)^2 = \begin{cases} \geq 1 & \text{failure} \\ < 1 & \text{no failure} \end{cases} \quad (6)$$

where  $X^T$  is a longitudinal tensile strength,  $X^C$  is a longitudinal compressive strength,  $Y^T$  is a transverse tensile strength and  $Y^C$  is a transverse compressive strength. For damage evolution, both models; anisotropic yield criteria with ductile damage for KFRP and Hashin damage for CFRP share the same softening law. After damage initiation, behavior degradation in each failure mode is characterized by energy dissipation using a linear softening law denoted by  $G_f$  (eq.7) [4].

$$G_f = \int_{\varepsilon_{eq}^{pl} at i}^{\varepsilon_{eq}^{pl} at f} L \sigma_{eq}^i d\varepsilon_{eq}^{pl} = \int_0^{\delta_j^{pl}} \sigma_{eq}^i d\delta^{pl} \quad (7)$$

where  $L$  is the characteristic length of elements,  $\sigma_{eq}^i$  is equivalent stress at damage initiation,  $\varepsilon_{eq}^{pl}$  is equivalent plastic strain, and  $\delta^{pl}$  is plastic displacement. Since this energy dissipation depends on each failure mode, the four different values of energy dissipation for Hashin damage were expected. The mechanical properties of KFRP and CFRP composite are summarized in Table I and II respectively. Most of properties were identified by tensile tests except an energy dissipation,  $G_f$ . This property was identified by a coupling of numerical simulations with experimental results from drop-weight impact test mentioned later in the FEM simulations section.

TABLE I. PROPERTIES OF CFRP COMPOSITE WITH EPOXY RESIN [5]

Density	1600 kg/m <sup>3</sup>
Elastic	$E_{11} = 14056.8MPa; E_{22} = 14056.8MPa;$ $E_{33} = 1948MPa; \nu_{12} = 0.08; \nu_{13} = 0.698;$ $\nu_{23} = 0.698; G_{12} = 1132MPa; G_{13} = 1100MPa;$ $G_{23} = 1100MPa$
Plasticity	$\sigma_{yield} = A(\varepsilon_{eq}^p)^3 + B(\varepsilon_{eq}^p)^2 + C\varepsilon_{eq}^p + D$ $A = 1040.1MPa; B = 821MPa; C = 366.9MPa;$ $D = 49.6MPa$
Plasticity Potential	$R_{11} = 1; R_{22} = 1; R_{33} = 1.89; R_{12} = 0.56;$ $R_{13} = 1.91; R_{23} = 1.91$
Ductile Damage	$\varepsilon_{eq}^p at i = 0.018$
Damage Evolution	$G_f = 5N / mm$

TABLE II. MECHANICAL PROPERTIES OF CFRP COMPOSITE [6]

Density	1650 kg/m <sup>3</sup>
Elastic	$E_{11} = 42749.6MPa; E_{22} = 42749.6MPa;$ $E_{33} = 3500MPa; \nu_{12} = 0.04; \nu_{13} = 0.38;$ $\nu_{23} = 0.38; G_{12} = 2940.8MPa;$ $G_{13} = 1250MPa; G_{23} = 1250MPa$
Hashin Damage	$X^T = 512.3MPa; X^C = 330MPa$ $Y^T = 512.3MPa; Y^C = 330MPa$ $S^T = 76.8MPa; S^L = 76.8MPa$
Damage Evolution	$G_{f,L}^T = G_{f,L}^C = G_{f,T}^T = G_{f,T}^C = 0.01N/mm$

For KFRP-CFRP composite, the delamination mode is obvious at the interface between different materials. This mode was expected since the interface of different materials will always weaker than the one from the same material due to the fact that the dissimilar of behaviors induced higher local stress concentration at interface. As mentioned previously, the prediction of delamination cannot be done by the 2D Hashin failure due to the lack of out-of-plane stresses. Thus, the concept of cohesive zone model is a good candidate to solve these difficulties. The cohesive elements were implemented in the finite element model to represent an epoxy layer at the interface between KFRP and CFRP. For coupled traction-separation behavior, the stress-strain relationship is written as follows [4]:

$$\begin{Bmatrix} t_n \\ t_s \\ t_t \end{Bmatrix} = \begin{bmatrix} k_n & 0 & 0 \\ 0 & k_s & 0 \\ 0 & 0 & k_t \end{bmatrix} \begin{Bmatrix} \varepsilon_n \\ \varepsilon_s \\ \varepsilon_t \end{Bmatrix} \quad (8)$$

where  $t_n, t_s$  and  $t_t$  are stresses in normal and two local shear directions,  $\varepsilon_n, \varepsilon_s$  and  $\varepsilon_t$  represent the corresponding strains and  $k_n, k_s$  and  $k_t$  are corresponding penalty stiffnesses. The onset of damage is introduced by QUADS damage [4], a damage initiation based on the traction-interaction criterion for cohesive elements (eq.9).

$$\left(\frac{t_n}{t_n^0}\right)^2 + \left(\frac{t_s}{t_s^0}\right)^2 + \left(\frac{t_t}{t_t^0}\right)^2 = \begin{cases} \geq 1 & \text{failure} \\ < 1 & \text{no failure} \end{cases} \quad (9)$$

where  $t_n^0, t_s^0$  and  $t_t^0$  are the maximum normal stress, in-plane and out-of-plane shear stress respectively. According to fracture mechanics, brittle fracture failure modes can be categorized into three different modes depending on geometries and loading direction. The mode I is an opening mode while the others mode II & III are in-plane and out-of-plan shear modes respectively. In this study, the mixed mode fracture energy with Benzeggagh-Kenane (BK) linear softening [7,8] is used for damage evolution of the cohesive zone. The critical fracture energy for BK criterion is written as in eq.10 [4]. This criterion considers that the critical fracture energies

during deformation along the first and the second shear directions (mode II & III) are the same, thus  $G_{IIC} = G_{IIIc}$ .

$$G_C = G_{IC} + \left( (G_{IIC} - G_{IC}) + (G_{IIIc} - G_{IIC}) \left( \frac{G_{III}}{G_{II} + G_{III}} \right) \right) \left( \frac{G_{II} + G_{III}}{G_I + G_{II} + G_{III}} \right)^\eta \quad (10)$$

where  $G_{IC}$  and  $G_{IIC}$  are the critical fracture energy in mode I and II, and  $\eta$  is a material parameter. An example of a traction elastic and linear softening triangular constitutive response of the cohesive zone is shown in Fig. 2 and the mechanical interface properties of epoxy resin for delamination failure is summarized in Table III.

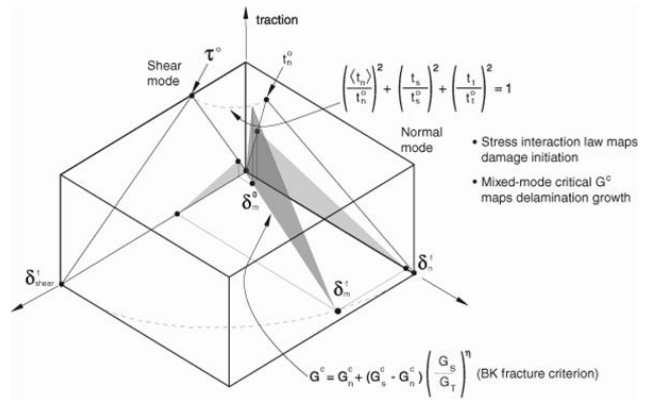


Figure 2. Mixed-mode response in cohesive element [4]

TABLE III. MECHANICAL INTERFACIAL PROPERTIES OF EPOXY [9]

Density	1400 kg/m <sup>3</sup>
Penalty stiffness	$k_n = k_s = k_t = 10^6 MPa$
Quads Damage	$t_n^0 = 30MPa; t_s^0 = t_t^0 = 60MPa$
Damage Evolution •BK criterion	$G_{IC} = 0.2 N/mm; G_{IIC} = G_{IIIc} = 0.6 N/mm;$ $\eta = 1$

### III. DROP-WEIGHT IMPACT TEST

The drop-weight impact test in this study is based on ASTM-D7136 standard. The corresponding specimen sizes and the test rig setup are shown in Fig.3. Three type of specimens were tested including KFRP, CFRP and KFRP-CFRP composite plates with the thickness of 2.8, 2.54 and 2.73 mm respectively. The concept is to maintain the plate thickness. The very thick plates cannot be tested due to the limit of drop-weight machine. Since the thickness of Kevlar and carbon ply is not the same so that KFRP specimen contains 4-plyes of Kevlar, CFRP specimens contain 8-plyes of carbon and KFRP-CFRP specimen contains 2-plyes of Kevlar and 4 plyes of carbon. The impact energies vary though the height of impactor at 400, 500, 600, 700 and 800 mm with a constant impactor weight of 5.87 kg. The velocity before and after impact were estimated from high speed camera using a pixel-count image analysis technique. This method provides more accurate velocity than direct conversion from

dropping height since it cancels out a friction effect of the impactor guiding column. The test results are summarized in Table IV. Concerning to the failure surfaces (Fig.4), the KFRP composite has a circular shape of impactor with fiber breaks at the end. This failure surface indicates a ductile damage. For the CFRP composite, the failure surface shows a cross-shaped crack which is clearly a brittle damage. The KFRP-CFRP composite shows a mix of both with an additional delamination between a layer of different material. It seems that the delamination isolated KFRP and CFRP plies then each material undergoes its own damage. This mechanism will be numerically confirmed in the following section.

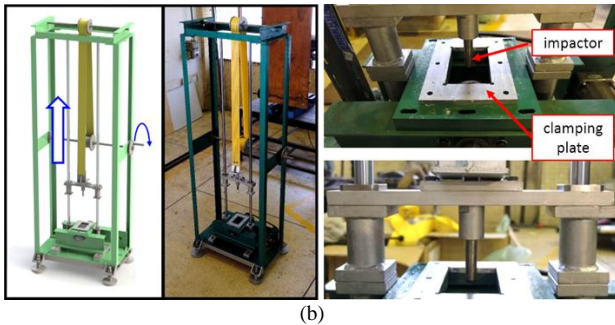
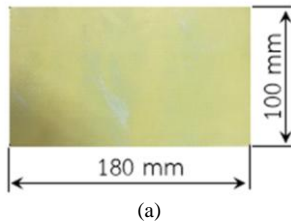


Figure 3. Drop-weight impact test: (a) test specimen, (b) experimental setup

TABLE IV. SUMMARY OF DROP-WEIGHT IMPACT TEST RESULTS

Material	Thickness (mm)	Height (mm)	Mean velocity before impact (mm/s)	Mean velocity after impact (mm/s)	Perforation
KFRP composites	2.8	700	3179	1735	No
		800	3349	1799	Yes/No
CFRP composites	2.54	500	2780	1304	No
		600	3089	-	Yes
CFRP-KFRP composites	2.73	400	2555	947	No
		500	2902	763	Yes/ No
		600	3155	-	Yes

\*\*Yes/No = mix of perforation results (3 specimens per height)

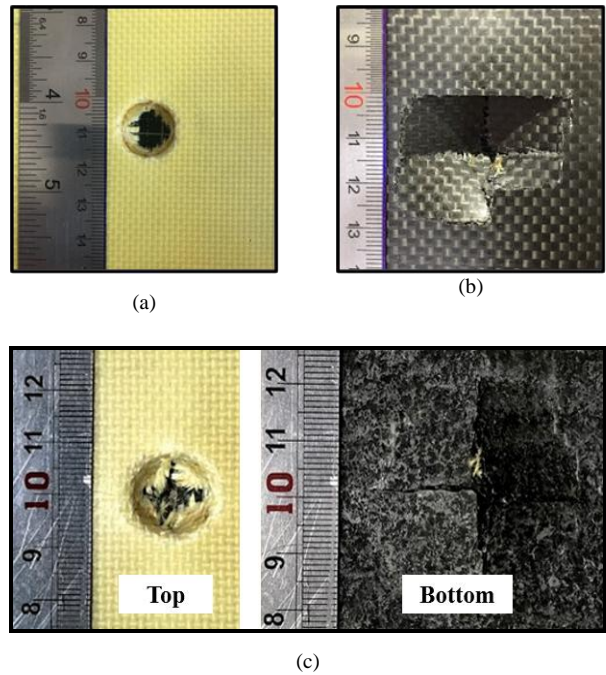


Figure 4. Failure surface: (a) KFRP composite plate, (b) CFRP composite, (c) KFRP-CFRP composite

#### IV. FEM SIMULATIONS

The FEM simulations of drop-weight impact test were carried out using ABAQUS, a finite element commercial software. All type of composite laminates in this study were involved with different objectives. The KFRP and CFRP composites simulations are for identification of their fracture energy mentioned previously while the simulation of KFRP-CFRP composite validates the damage models presented in this work to simulate its failure surface. The numerical specimens were modelled using continuum shell elements (SC8R) for KFRP and CFRP plies. The size of elements is crucial and needs to be consisted thought out the impact zone. The size of 2x2 mm<sup>2</sup> was selected. This value was also treated as a characteristic length (2 mm) for fracture energy so that the identified value was restricted to this length. When apply to KFRP-CFRP composite simulation, the element size of 2x2 mm<sup>2</sup> has to be fixed at the impact zone in order to use the corresponding fracture energy. In addition to KFRP-CFRP composite simulation, the cohesive elements (COH3D8) were used to represent the epoxy interface layer of different material. The interfacial thickness was set to 0.06 mm. The steel impactor was assigned as a non-deformable rigid body using shell element to reduce the number of elements. Its impact velocity was applied according to Table IV. The border of specimen was fixed in all direction as it was clamped by the clamping plate in the real test. Fig.5 shows a finite element model and its meshed version.

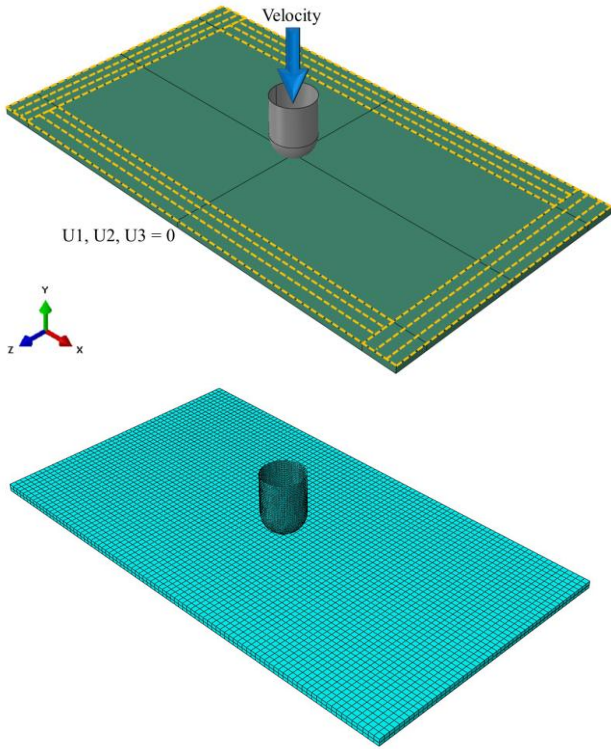


Figure 5. Finite element model of drop weight impact test

In order to identify the fracture energy per unit area ( $G_f$  in N/mm), the simulations were performed at the velocity where the composite plates were perforated which is 3349 mm/s or 800 mm in height for KFRP composite and 3089 mm/s or 600 mm in height for CFRP composite. The simulation results are illustrated in Fig.6 and 7 respectively. The removed element option in ABAQUS was activated to hide the failure elements for more realistic visualizations. From the top and side view of both cases, the failure surfaces show a sign of ductile for KFRP composite and brittle for CFRP composite as in the experimental results (Fig.4). The fracture energy per unit area was identified at 5 N/mm for KFRP composite and 0.01 N/mm for CFRP composite as summarized in Table I&II. With all mechanical properties, the simulations of tensile test were additionally performed as a validation. The comparison of simulation to experimental results is shown in Fig.8 for both KFRP and CFRP composites.

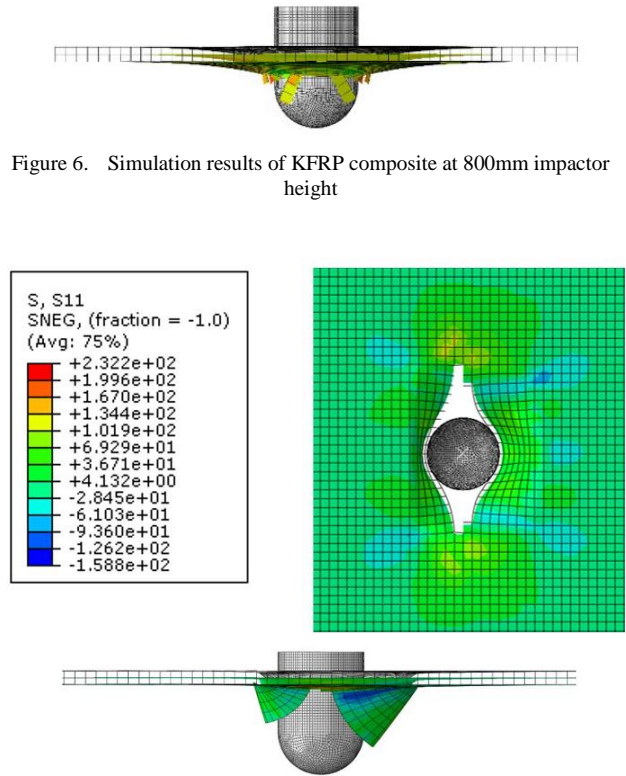
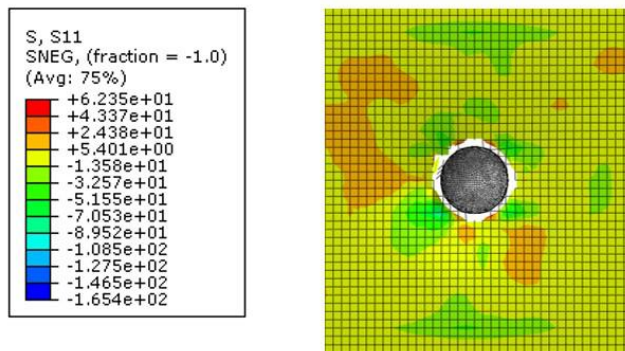


Figure 6. Simulation results of KFRP composite at 800mm impactor height

Figure 7. Simulation results of CFRP composite at 600mm impactor height

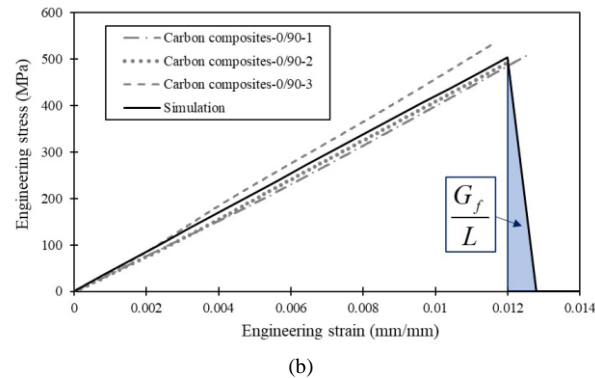
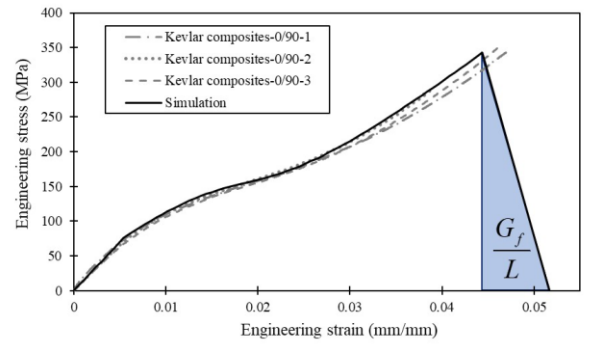


Figure 8. Tensile test simulation results for the validation of mechanical properties: (a) KFRP composite, (b) CFRP composite

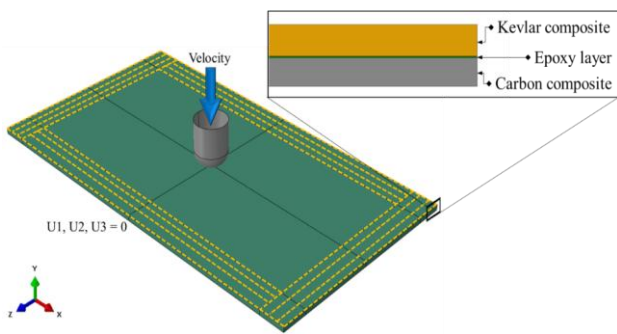


Figure 9. KFRP-CFRP composite model with epoxy layer

The drop-weight impact test on KFRP-CFRP composite was finally simulated at the height of 400 and 500 mm. As mentioned, the epoxy layer was insert between KFRP and CFRP as an interface layer (Fig.9). From damage observation, the failure was initiated by the delamination at cohesive element layer illustrated by the element deletion (Fig.10). This delamination isolated the KFRP and CFRP plies. As a result, each ply undergoes its own damage which is ductile for KFRP and brittle for CFRP. This mechanism also observed from the tested specimens. Concerning to the results from different height of impactor, at 400 mm the perforation was not occurred since the impactor bounced back from the plate after impact (Fig.11). However, the plate was visibly damaged. This height can be considered as the limit of composite plate to withstand the perforation. The experimental results also confirmed this conclusion where some of specimen was perforated and some of them are not. The perforation was clear at 500 mm impactor height (Fig.12) with a mix of damage mechanisms as described. This also had a good agreement with experiments where all the tested specimens were perforated at this height.

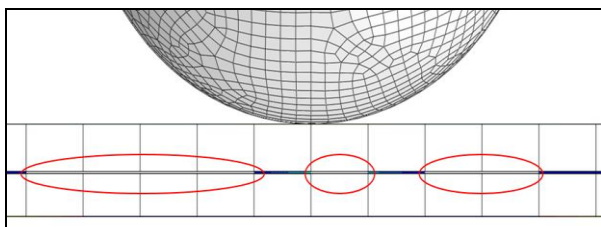


Figure 10. Cohesive elements failure indicated by deleted elements (in red)

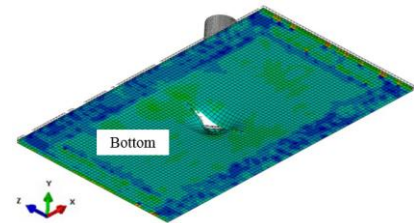
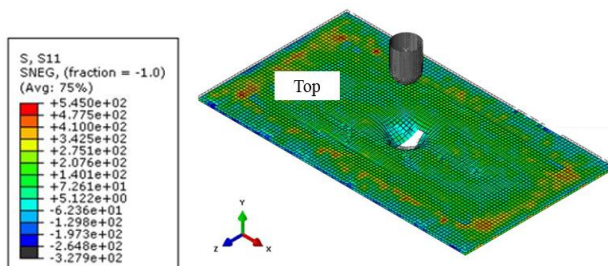


Figure 11. Simulation results of KFRP-CFRP composite at 400 mm impactor height

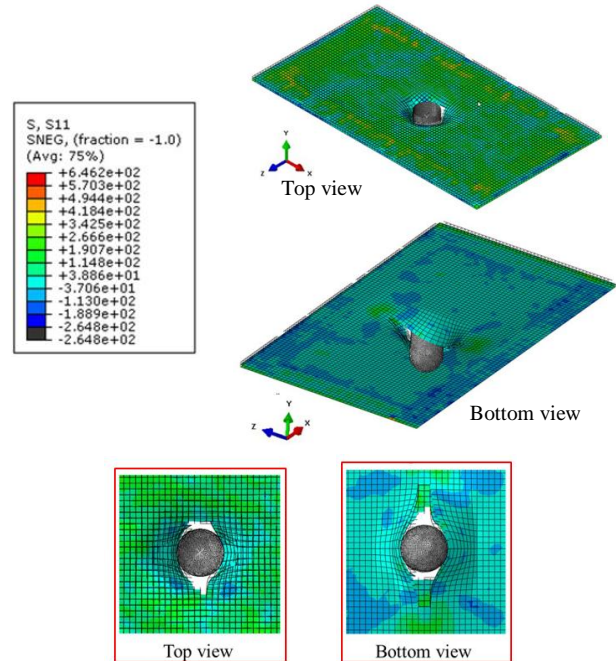


Figure 12. Simulation results of KFRP-CFRP composite at 500 mm impactor height

## V. CONCLUSION

The damage investigation on KFRP/CFRP composite laminates under low-velocity impact reveals some interested mechanism. For the combination of different material, the strength of interface is a key parameter since the behavior gradient induces a higher stress concentration at interface than other zones. The delamination of this interface will isolate each material and make them lose their advantages as the case of this study. The purpose of KFRP-CFRP composite is to improve the impact resistance of CFRP using KFRP plies but with the onset of delamination, the impact resistance is roughly the same when compare to CFRP composite. The gain in strength of interface will delay the onset of delamination which certainly improve the impact resistance of KFRP-CFRP composite. Considering the numerical aspect, the finite element model with various of damage models including the anisotropic yield criterion with ductile damage for KFRP plies, Hashin damage model for CFRP and BK damage model for epoxy interfacial layer is capable to interpret the damage in composite materials. The simulation results had a good agreement with experiments in term of failure surface.

For future work, the energy absorption can also be investigated numerically since the high-speed camera provided the velocity before and after impact. In case of non-perforation, this quantity will rely especially on the degraded elastic behavior of materials which affect directly to the parameter of current FEM model.

#### CONFLICT OF INTEREST

The authors declare no conflict of interest.

#### AUTHOR CONTRIBUTIONS

Mr. Kerati Suwanpakpraek as first author to conduct the research under the supervision of Asst. Prof. Dr. Baramee Patamaproh (corresponding author), a head of the research project, who finalized a manuscript. Two authors contributed in writing the manuscript and had approved the final version.

#### ACKNOWLEDGMENT

This research is supported by the Science and Technology Research Institute (STRI) at King Mongkut's University of Technology North Bangkok through the project entitled "Study of composite behavior and damage under low-velocity impact loading", grant no. KMUTNB-64-NEW-07.

Special thanks are given to Asst. Prof. Dr. Pongsak Nimdum, a mentor of this project and also a head researcher of the project entitled "Feasibility study of lightweight composite helmet for Thai skull morphology" granted by the Office of the Higher Education Commission (OHEC). All experimental data are brought from this project.

#### REFERENCES

- [1] G. Daniel and S. V. Hoa, *Composite Materials: Design and Applications*, CRC press, 2007.
- [2] R. Bogenfeld, J. Kreikemeier, and T. Wille, "Review and benchmark study on the analysis of low-velocity impact on composite laminates," *Engineering Failure Analysis*, vol. 86, pp. 72-99, 2018.
- [3] B. Jean-Marie, "Composite materials: Mechanical behavior and structural analysis," *Nisan 1997*, 2018.
- [4] Hibbit, Karlsson, and Sorensen, "ABAQUS theory manual, version 5.5," 1995.

- [5] M. Rodríguez-Millán, T. Ito, J. A. Loya, A. Olmedo, and M. H. Miguñez, "Development of numerical model for ballistic resistance evaluation of combat helmet and experimental validation," *Materials & Design*, vol. 110, pp. 391-403, 2016.
- [6] T. Kanketr, E. Phongphinnittana, and B. Patamaproh, "Design of a CFRP composite monocoque: simulation approach," in *Proc. IOP Conference Series: Materials Science and Engineering*, vol. 501, no. 1, pp. 012014, 2019.
- [7] J. Choothum, "Kissing bonds in adhesive joints: a holistic approach for surface chemistry and joint mechanics," Ph.D. dissertation, Dept. Engineering and Materials Science, Queen Mary, University of London, 2011.
- [8] M. O. Bozkurt, L. Parnas, and D. Coker, "Simulation of drop-weight impact test on composite laminates using finite element method," *Procedia Structural Integrity*, vol. 21, pp. 206-214, 2019.
- [9] J. Xue, W. X. Wang, J. Z. Zhang, S. J. Wu, "Progressive failure analysis of the fiber metal laminates based on chopped carbon fiber strands," *Journal of Reinforced Plastics and Composites*, vol. 34, pp. 364-376, 2015.

Copyright © 2022 by the authors. This is an open access article distributed under the Creative Commons Attribution License (CC BY-NC-ND 4.0), which permits use, distribution and reproduction in any medium, provided that the article is properly cited, the use is non-commercial and no modifications or adaptations are made.



**Kerati Suwanpakpraek** is a Ph.D. student in mechanical engineering from King Mongkut's University of Technology North Bangkok, Thailand. He received a bachelor of engineering degree in mechanical engineering from the same university in 2016. His research interests include composites, adhesives, computer modelling and finite element analysis.



**Baramee Patamaproh** is currently an assistant professor at the Department of Mechanical and Aerospace Engineering, King Mongkut's University of Technology North Bangkok, Thailand. He received his Ph.D. in materials science and engineering from Mines ParisTech, France in 2014. From 2014-2016, he was a post-doctoral researcher for the study of mechanical characterisation of multi-material assembly and behaviour modelling at Centre des matériaux, Mines ParisTech, France. His research interests include composites, adhesives, multi-material joining and finite element Analysis.